2013

Using Ammonium Pore Water Profiles to Assess Stoichiometry of Deep Remineralization Processes in Methanogenic Continental Margin Sediments

David J. Burdige
Old Dominion University, dburdige@odu.edu

Tomoko Komada

Original Publication Citation

Burdige, D.J., & Komada, T. (2013). Using ammonium pore water profiles to assess stoichiometry of deep remineralization processes in methanogenic continental margin sediments. *Geochemistry Geophysics Geosystems, 14*(5), 1626-1643. doi: 10.1002/ggge.20117

Geochemistry Geophysics Geosystems G3

Volume 14, Number 5
29 May 2013
doi:10.1002/ggge.20117
ISSN: 1525-2027

Published by AGU and the Geochemical Society

Using ammonium pore water profiles to assess stoichiometry of deep remineralization processes in methanogenic continental margin sediments

David J. Burdige
Department of Ocean, Earth and Atmospheric Sciences, Old Dominion University, Norfolk, Virginia, 23529, USA (dburdige@odu.edu)

Tomoko Komada
Romberg Tiburon Center, San Francisco State University, Tiburon, California, USA

[1] In many continental margin sediments, a deep reaction zone exists which is separated from remineralization processes near the sediment surface. Here, methane diffuses upward to a depth where it is oxidized by downwardly diffusing sulfate. However, the methane sources that drive this anaerobic oxidation of methane (AOM) in the sulfate-methane transition zone (SMT) may vary among sites. In particular, these sources can be thought of as either (i) "internal" sources from in situ methanogenesis (regardless of where it occurs in the sediment column) that are ultimately coupled to organic matter deposition and burial, or (ii) "external" sources such as hydrocarbon reservoirs derived from ancient source rocks, or deeply buried gas hydrates, both of which are decoupled from contemporaneous organic carbon deposition at the sediment surface. Using a modeling approach, we examine the relationship between different methane sources and pore water sulfate, methane, dissolved inorganic carbon (DIC), and ammonium profiles. We show that pore water ammonium profiles through the SMT represent an independent "tracer" of remineralization processes occurring in deep sediments that complement information obtained from profiles of solutes directly associated with AOM and carbonate precipitation, i.e., DIC, methane, and sulfate. Pore water DIC profiles also show an inflection point in the SMT based on the type of deep methane source and the presence/absence of accompanying upward DIC fluxes. With these results, we present a conceptual framework which illustrates how shallow pore water profiles from continental margin settings can be used to obtain important information about remineralization processes and methane sources in deep sediments.

Components: 10,385 words, 6 figures, 6 tables.

Keywords: anaerobic oxidation of methane; sediment biogeochemistry.

Index Terms: 4804 Oceanography: Biological and Chemical (0460): Benthic processes, benthos (0408); 4802 Oceanography: Biological and Chemical (0460): Anoxic environments (0404, 1803, 4834, 4902); 4806 Oceanography: Biological and Chemical (0460): Carbon cycling (0428); 4805 Oceanography: Biological and Chemical (0460): Biogeochemical cycles, processes, and modeling (0412, 0414, 0793, 1615, 4912); 4825 Oceanography: Biological and Chemical (0460): Geochemistry.

Received 6 December 2012; **Revised** 12 March 2013; **Accepted** 12 March 2013; **Published** 29 May 2013.

Burdige, D. J., and T. Komada (2013), Using ammonium pore water profiles to assess stoichiometry of deep remineralization processes in methanogenic continental margin sediments, *Geochem. Geophys. Geosyst.*, *14*, 1626–1643, doi:10.1002/ggge.20117.

1. Introduction

[2] Both qualitative [*Cowie and Hedges*, 1994] and quantitative [*Middelburg*, 1989] observations suggest that under steady state conditions, organic matter reactivity decreases with increasing age. In sediments, where age increases with sediment burial, organic matter reactivity generally decreases with depth because more labile organic matter is preferentially remineralized near the sediment surface, leaving behind less reactive organic matter for subsequent decomposition with burial. Organic matter remineralization rates are therefore generally highest near the sediment-water interface and decrease in a near-continuous fashion with depth [e.g., *Soetaert et al.*, 1996; *Martin and Sayles*, 2003; *Jørgensen and Parkes*, 2010]. In some marine sediments, however, profiles of pore water solutes such as O_2, nitrate, and sulfate suggest the occurrence of this type of depth attenuation of remineralization processes in surface sediments, along with the existence of a deeper reaction zone. Additionally, these two zones are separated by distances ranging from approximately tens of centimeters to meters, where the occurrence of linear pore water profiles implies the existence of an intermediate no-reaction, diffusion-dominated zone [e.g., *Goloway and Bender*, 1982; *Wilson et al.*, 1985; *Niewöhner et al.*, 1998; *Borowski et al.*, 1999; *Berelson et al.*, 2005]. There are, however, several caveats to this explanation. For example, linear profiles can also be obtained when there are low rates of remineralization in this intermediate region as compared to higher rates in the overlying and underlying sediments [*Burdige and Komada*, 2011]. Similarly, curvature in sediment pore water profiles does not necessarily imply nonconservative solute behavior if there is significant pore-water advection, or if there are significant changes in diffusion coefficients with depth due to temperature and/or porosity variations [*Lerman*, 1977; *Dickens*, 2001].

[3] These factors notwithstanding, the causes of this apparent uncoupling between surface sediment remineralization processes and those in a deep reaction zone are not well understood and may vary among different sedimentary settings. For example, in some pelagic and hemipelagic settings, this can be the result of turbidite deposition and diagenesis [e.g., *Goloway and Bender*, 1982; *Sørensen et al.*, 1984; *Wilson et al.*, 1985]. Here the gravity-driven flow of relatively organic-rich continental margin sediments onto organic-poor sediments sets up a situation in which the subsequent burial and remineralization of organic matter in the turbidite results in a subsurface reaction front for aerobic respiration, denitrification, and metal redox cycling [also see a review in *Burdige*, 2006].

[4] In many other continental margin sediments, the apparent uncoupling is due to the occurrence of a deep reaction zone at the transition between sulfate-reducing and methanogenic sediments. In this sulfate-methane transition zone (SMT), sulfate concentrations go to zero as methane diffuses (or is advected) upward to the SMT where it is oxidized by downwardly diffusing sulfate, through a microbially mediated process termed anaerobic oxidation of methane, or AOM [*Reeburgh*, 2007; *Knittel and Boetius*, 2009]:

$$CH_4 + SO_4^{2-} \rightarrow HS^- + HCO_3^- + H_2O \quad (1)$$

[5] In different continental margin settings, the depth of the SMT may vary from less than a meter below the sediment surface to ~10–20 m or more [*Iversen and Jørgensen*, 1985; *Niewöhner et al.*, 1998; *Borowski et al.*, 1999; *Dickens*, 2001; *D'Hondt et al.*, 2002; *Hensen et al.*, 2003; *Berelson et al.*, 2005; *Snyder et al.*, 2007; *Knab et al.*, 2008; *Chatterjee et al.*, 2011; *Malinverno and Pohlman*, 2011; and others]. The SMT not only represents a discrete zone of AOM activity, but is also an important site of iron sulfide mineral precipitation [*Hensen et al.*, 2003; *Borowski et al.*, 2013]. In addition, because AOM produces alkalinity, it can also be a site of extensive carbonate precipitation [*Berelson et al.*, 2005; *Meister et al.*, 2007; *Snyder et al.*, 2007].

[6] Past studies of these systems have tended to focus on interpreting processes in the SMT by examining the concentration and isotopic composition of solutes directly associated with AOM and carbonate precipitation, i.e., dissolved inorganic carbon (DIC), methane, and sulfate (see references cited above). However, a number of fundamental questions remain, including the relationship between the origin of the methane that drives AOM and the resulting pore water profiles of associated solutes.

[7] Previously, we used a modeling approach to examine how pore water profiles of sulfate, methane, and DIC can be used to infer whether methane involved in AOM is produced locally by methanogenesis, or is introduced from a source at depth that is decoupled from ongoing organic matter degradation, such as geologic hydrocarbon reservoirs and/or deeply buried

gas hydrate deposits [*Burdige*, 2011; *Burdige and Komada*, 2011]. Recent modeling efforts have also examined similar aspects of this problem [*Chatterjee et al*., 2011; *Malinverno and Pohlman*, 2011; *Meister et al*., 2013].

[8] Here we continue to examine this problem using an expanded version of the reactive-transport model described in *Burdige and Komada* [2011] that also allows us to examine ammonium pore water profiles. Ammonium profiles that penetrate through the SMT have been reported in the literature [*Borowski et al*., 1996; *Niewöhner et al*., 1998; *Borowski and Paull*, 2000], but their relationship to methane biogeochemistry in deep sediments has not been fully explored. We address this knowledge gap by specifically linking the upward flux of methane to the SMT to processes that may also produce DIC and ammonium below the SMT. Specifically, we show that pore water ammonium profiles through the SMT represent an independent "tracer" of remineralization processes occurring in deep sediments that complement information obtained solely from profiles of DIC, methane, and sulfate. Through an examination of this problem using model sediment systems, we develop a conceptual framework that illustrates how surface pore water profiles can be used to obtain important information about remineralization processes and methane sources in deep marine sediments.

2. Background

[9] In coastal or nearshore marine sediments, sulfate reduction and methanogenesis generally occur in the upper several meters or less of sediment [*Burdige*, 2006]. Methanogenesis occurs immediately below the zone of sulfate reduction, once pore water sulfate is completely, or near-completely, consumed [*Reeburgh*, 2007; *Alperin and Hoehler*, 2009], consistent with the "classic" biogeochemical zonation model [*Claypool and Kaplan*, 1974; *Froelich et al*., 1979]. Overall, the depth distribution of sulfate reduction and methanogenesis in this model is primarily driven by the deposition and burial of reactive particulate organic matter, and this methanogenesis is the primary source of methane for the AOM that occurs in the SMT. In such sediments, AOM generally represents less than ~30% of the total sulfate reduction [*Reeburgh*, 1983; *Devol et al*., 1984; *Iversen and Jørgensen*, 1985; *Martens et al*., 1998; *Dale et al*., 2008], and for coastal and nearshore sediments globally, an average value of ~12% appears to be reasonable [*Henrichs and Reeburgh*, 1987]. Thus in these sediments, sulfate reduction directly tied to the oxidation of reactive particulate organic matter generally dominates over AOM.

[10] In contrast, in some continental margin sediments, sulfate reduction over the entire sediment column may be dominated by AOM in the SMT. Here sulfate profiles are linear, or near-linear, from the sediment surface to the SMT, suggesting the dominance of diffusive transport of sulfate throughout the sediment column above the SMT [e.g., *Niewöhner et al*., 1998; *Borowski et al*., 1999; *Berelson et al*., 2005; *Burdige*, 2011]. However, the sources of the methane that drives AOM in these continental margin sediments are not well characterized. In the discussion below, we separate the methane sources broadly into those that we refer to as "internal" and "external."

2.1. Internal Methane Sources for AOM in Continental Margin Sediments

[11] Much of the methane that drives AOM in continental margin sediments is not necessarily produced just below the SMT, as it is in many nearshore and coastal sediments. Rather, it may be produced in a deep zone of methanogenesis, some tens to hundreds of meters below the SMT. The causes of this relatively large spatial separation between the SMT and a deeper zone of active methanogenesis are not well understood [*Wellsbury et al*., 1997; *Wallmann et al*., 2006; *Burdige*, 2011; *Archer et al*., 2012], and discussion of this problem is beyond the scope of this paper. Nevertheless, regardless of this consideration, we can think of this deep in situ methanogenesis as ultimately being coupled to organic matter deposition at the surface and its subsequent burial. Furthermore, this methane is largely transported by vertical diffusion from its depth of production to its depth of consumption. We refer to this as an "internal" deep source of methane.

[12] In settings where methane is derived from such a deep internal source, there will be concomitant DIC production as well as ammonium and phosphate production during the complete remineralization of sedimentary organic matter by the consortium of anaerobes (i.e., hydrolytic, fermentative as well as methanogenic microbes) that mediate the process [*Megonigal et al*., 2003; *Burdige*, 2006]. The overall process by which this biogenic methane is produced can be expressed as

$$(C_{org})_x(NH_3)_y(H_3PO_4)_z \rightarrow xL_2CH_4 + xL_3CO_2 + yNH_3 + zH_3PO_4 \quad (2)$$

where C_{org} is reactive particulate organic carbon (also referred to here as POC), L_2 is the molar

Table 1. A List of Abbreviations Used in the Model Equations

Symbol	Definition
Solutes and Solids	
C	DIC (dissolved inorganic carbon)
G	Reactive particulate organic carbon (POC) in sediments
N	Ammonium
S	Sulfate
Other Parameters	
D_{si}	The bulk sediment diffusion coefficient for solute i (corrected for temperature and sediment tortuosity as discussed in Table 3)
F	A factor that converts solid phase concentration units to pore water solute concentration units [*Burdige*, 2006]
f_S	A function that inhibits the occurrence of methanogenesis when sulfate concentrations are above some threshold value [*Burdige*, 2011]
gdw	Grams dry weight (in units for reactive POC in sediments)
$J_{lb,i}$	Upward flux of solute i at the lower model boundary
k_i	Rate constant for organic matter remineralization ($i = OM$) or AOM ($i = aom$)
K_m	Half-saturation constant for sulfate reduction
L_2 [a]	Moles of CH_4 produced per mole of C_{org} oxidized during methanogenesis
L_3 [a]	Moles of DIC (expressed as CO_2), produced per mole of C_{org} oxidized during methanogenesis
ox	Carbon oxidation state in C_{org}
φ	Sediment porosity
ω	The sediment accumulation rate (and the rate of pore water advection driven by sedimentation, since we have implicitly assumed that sediment porosity is constant with depth)
$r_{N:C}$ [a]	Nitrogen:carbon ratio of organic matter undergoing remineralization
$r_{C:S}$	Moles of C_{org} oxidized, or DIC produced, per mole of sulfate reduced during sulfate reduction

[a]Values of these parameters with the superscript "deep" are specifically for the organic matter undergoing remineralization by methanogenesis in deep sediments below the lower model boundary (e.g., see equations (5) and (6) and related discussions).

amount of CH_4 produced per mole of C_{org} oxidized, L_3 is the molar amount of DIC (expressed here as CO_2) produced per mole of C_{org} oxidized, and $x{:}y{:}z$ is the C:N:P ratio of this organic matter (we also specifically define the N:C ratio of this material as $r_{N:C}$ [$=y/x$]; see Table 1 for a list of all abbreviations). If we approximate C_{org} as CH_2O, then $L_2 = L_3 = \frac{1}{2}$, although for C_{org} whose carbon oxidation state (ox) does not equal zero, L_2 equals $(4 - ox)/8$ [*Burdige*, 2006], while L_3 equals $(4 + ox)/8$ [*Burdige and Komada*, 2011]. For the sake of simplicity, this equation is not completely balanced because we have not specified the bulk H:C and O:C ratios of C_{org}. Partial remineralization of C_{org} may also occur in conjunction with complete remineralization and similarly lead to ammonium, DIC, and phosphate production along with production of a broad range of dissolved organic carbon (DOC) compounds in addition to CO_2 [see, for example, *Kujawinski*, 2011]. However, expressing partial C_{org} remineralization with a defined stoichiometry such as that in equation (2) is difficult, because of the complexity of the different types of fermentation reactions observed in nature [e.g., *Thauer et al.*, 1977], and because of the wide range of DOC compounds that can be produced during microbial remineralization.

[13] Expressing sulfate reduction in a similar fashion yields

$$\left(C_{org}\right)_x\left(NH_3\right)_y\left(H_3PO_4\right)_z + \frac{x}{r_{C:S}}SO_4^{2-} \rightarrow xHCO_3^- + \frac{x}{r_{C:S}}HS^- + yNH_3 + zH_3PO_4 \quad (3)$$

where $r_{C:S}$ is the molar amount of C_{org} oxidized, or DIC produced, per mole of sulfate reduced. When C_{org} is approximated as CH_2O, $r_{C:S} = 2$ and in general, $r_{C:S}$ equals $8/(4 - ox)$ for C_{org} whose carbon oxidation state is ox [*Burdige*, 2006]. Analogous to methanogenesis, sulfate reduction is mediated by a consortium of hydrolytic, fermentative, and sulfate-reducing anaerobes.

2.2. External Methane Sources for AOM in Continental Margin Sediments

[14] Methane that is oxidized in the SMT may also be derived from a deep "external" source that unlike the internal sources described above, is decoupled from contemporaneous organic matter deposition at the sediment surface followed by remineralization and burial. External methane sources might include hydrocarbon reservoirs derived from ancient source rocks, or deeply buried gas hydrate deposits [see discussions and references in *Burdige and Komada*, 2011]. Furthermore, such an external methane source in a given sediment setting may actually have been

Table 2. Model Equations[a]

Pore water sulfate (*S*)	$0 = D_{sS}\frac{\partial^2 S}{\partial z^2} - \frac{1}{r_{S:C}}\frac{k_{OM}FGS}{K_m+S} - k_{\mathrm{aom}}SM$
	[diffusion; C_{org} remineralization driven by sulfate reduction (equation (3)); and anaerobic oxidation of methane (equation (1))]
Reactive POC (*G*)	$0 = -\omega\frac{\partial G}{\partial z} - \frac{k_{OM}GS}{K_m+S} - f_S k_{OM} G$
	[advection driven by sedimentation; C_{org} remineralization driven by sulfate reduction (equation (3)); and C_{org} remineralization driven by methanogenesis (equation (2))]
Pore water methane (*M*)	$0 = D_{sM}\frac{\partial^2 M}{\partial z^2} + f_S k_{OM} L_2 FG - k_{\mathrm{aom}}SM$
	[diffusion; C_{org} remineralization driven by methanogenesis (equation (2)); and anaerobic oxidation of methane (equation (1))]
Pore water DIC (*C*)	$0 = D_{sC}\frac{\partial^2 C}{\partial z^2} + \frac{k_{OM}FGS}{K_m+S} + f_S k_{OM} L_3 FG + k_{\mathrm{aom}}SM$
	[diffusion; C_{org} remineralization driven by sulfate reduction (equation (3)); C_{org} remineralization driven by methanogenesis (equation (2)); and anaerobic oxidation of methane (equation (1))]
Pore water ammonium (*N*)	$0 = D_{sN}\frac{\partial^2 N}{\partial z^2} + \frac{r_{N:C}k_{OM}FGS}{K_m+S} + f_S r_{N:C} k_{OM} L_3 FG$
	[diffusion; ammonium production associated with C_{org} remineralization driven by sulfate reduction (equation (3)); ammonium production associated with C_{org} remineralization driven by methanogenesis (equation (2))]

[a]Processes on the right-hand side of each equation are explained in brackets below each equation. Terms used in the equations are defined in Table 1.

produced elsewhere and subsequently migrated either laterally or vertically in the gaseous phase to its current location [e.g., *Hein et al.*, 2006; *Normark et al.*, 2006]. Relevant to this discussion is that both of these scenarios should result in a situation in which an external methane flux observed today (due to biogenic methane production in the past) is decoupled from ammonium or DIC production that may have occurred in the past along with the production of this methane. Although stable isotope measurements argue that deep methane sources are generally biogenic rather than thermogenic in origin [e.g., *Bohrmann and Torres*, 2006; *Paull et al.*, 2008], discussions in *Snyder et al.* [2007] suggest that there can also be some decoupling between upward fluxes of thermogenic methane and fluxes of DIC and ammonium.

[15] Decoupling of upward methane fluxes derived in this fashion from DIC and ammonium fluxes requires that the removal of methane from saturated sediment pore waters into a gaseous phase does not also result in significant removal of DIC and ammonium as CO_2(g) and NH_3(g), respectively. Support for this assumption stems in part from the fact that at the pH of sediment pore waters (~7–8.2), DIC and ammonium exist predominantly as HCO_3^- and NH_4^+ ions, versus aqueous CO_2 or NH_3, respectively (also see footnote b in Table 3) [*Zeebe and Wolf-Gladrow*, 2001].

[16] Consistent with these arguments, studies of methane gas bubbles that form in shallow anoxic sediments [e.g., *Martens and Klump*, 1980; *Martens and Chanton*, 1989] show that these bubbles contain less than a few percent CO_2. Gas bubbles at the seafloor derived from natural hydrocarbon seeps also contain ~10% to <1% CO_2 [*Leifer et al.*, 2006; *Paull et al.*, 2008], although it is unclear whether this CO_2 derives from the original underlying gas reservoir, or is produced in situ by processes occurring as the gas ascends from depth in the seabed to the seafloor. Finally, *Claypool and Kvenvolden* [1983] report that CO_2 is in general a "minor" or "trace" component of natural gas in marine sediments. Equally important though is the fact that if the methane in sediment systems such as those studied here is derived from methane gas that has migrated either laterally or vertically from its original source of production, then any DIC or ammonium that may have been produced along with this methane will likely have been "left behind."

[17] In addition, hydrate formation is generally thought to exclude all dissolved ions such as, e.g., chloride [*Bohrmann and Torres*, 2006]. Thus, if biogenic methane produced by methanogenesis is trapped as solid hydrate, it is likely that HCO_3^- and NH_4^+ ions are similarly excluded from the hydrate structure. This exclusion means that when environmental conditions change and the hydrate becomes an active methane source in sediment systems such as those discussed here, there will be no accompanying upward flux of either DIC or ammonium.

Table 3. Common Model Parameters[a]

Parameters		Units
Bulk sediment diffusion coefficients ($D_{s,i}$) [b]		
sulfate	124.7	$cm^2\ yr^{-1}$
DIC	134.2 ($\pm$7.1)	$cm^2\ yr^{-1}$
methane	195.6	$cm^2\ yr^{-1}$
ammonium	239.8	$cm^2\ yr^{-1}$
K_m	0.5 [c]	$mmol\ L^{-1}$
φ	0.8	
ox	−0.7	
k_{aom}	100 [c]	$mmol^{-1}\ L\ yr^{-1}$

[a]See Table 2 for definitions of all parameters.
[b]Bulk sediment diffusion coefficients were determined using the modified Weissberg equation $D_s = D°/[1 - \ln(\varphi^2)]$ [*Boudreau*, 1997], where $D°$ is the seawater free solution diffusion coefficient. Values of $D°$ were obtained from *Schulz and Zabel* [2006] for an assumed bottom water temperature of 5°C. The free solution diffusion coefficient for DIC is a weighted average of the diffusion coefficients for HCO_3^-, CO_3^{2-}, and aqueous CO_2 based on their relative average composition ($\pm 1\sigma$) in pore water DIC from Santa Monica Basin sediments ($93.7 \pm 2.8\%$, $3.8 \pm 3.5\%$, and $3.5 \pm 2.1\%$, respectively). Note that the bulk sediment diffusion coefficients for sulfate, methane, and DIC reported in Table 1 of *Burdige and Komada* [2011] are incorrectly listed and in fact are seawater free solution diffusion coefficients.
[c]From *Burdige and Komada* [2011].

3. Model Description and Analysis

[18] The model used here is a steady-state reactive transport model for sulfate (*S*), DIC (*C*), methane (*M*), ammonium (*N*), and reactive particulate organic carbon, or POC (*G*). The model equations are listed in Table 2, and the terms used in the equations are listed in Table 1. In this model, we assume that there is only one type of reactive POC undergoing remineralization, since having multiple pools of POC with different relativities undergoing remineralization (i.e., a multi-*G* model) does not affect the conclusions presented here.

[19] In the model, we further assume that porosity is constant with depth. The inclusion of variable porosity (due to sediment compaction) in reactive-transport model calculations over depth scales ranging from tens to a few hundred centimeters results in concentration differences, relative to constant porosity calculations, that differ by less than 15% over the entire calculated profiles [*Lerman*, 1977; *Klump and Martens*, 1989; *Komada et al*., 2013; D. Burdige, unpublished results]. Over longer depth (and timescales), the effects of variable porosity may be more significant [*Dickens*, 2001], especially if one is interested in specifically fitting the model to field data. In such cases, the equations used here can be adapted as necessary to account for compaction and variable porosity [*Burdige*, 2011].

[20] A Peclet number analysis [*Boudreau*, 1997] indicates that for the model parameters used here (Table 3), diffusion dominates over pore water advection driven by sedimentation, allowing us to safely ignore advection terms in the solute equations in Table 2. In sediment systems where advection driven by sediment compaction or by other processes (e.g., thermally driven fluid flow) is more significant [e.g., *Luff and Wallmann*, 2003; *Buffett and Archer*, 2004; *Hensen and Wallmann*, 2005], the model equations used here can again be modified as needed [*Burdige*, 2011].

[21] The upper boundary condition for the model equations specifies the sulfate, DIC, methane, and ammonium concentrations at the sediment-water interface (zero for methane and ammonium, and bottom water values for DIC and sulfate) and fixes the reactive POC concentration at the sediment surface (G_o in Table 4). The lower boundary of the model is set to $z = 400$ cm. We chose this depth since it encompasses the SMT in the coastal and inner continental margin sediments we are most interested in examining here, but excludes the less well understood deep processes that ultimately represent the sources of methane, and perhaps DIC and ammonium at the lower boundary.

[22] We consider three sets of lower boundary conditions for *M*, *C*, and *N*. In the first case, we assume that there is no upward flux of methane across the lower model boundary (i.e., there is no deep external nor internal source of methane). This implies that $\partial M/\partial z = \partial C/\partial z = \partial N/\partial z = 0$ at the lower boundary and is referred to here as the "no methane flux" lower boundary condition. In the second case, we prescribe an upward flux of methane across the lower model boundary ($J_{lb,m}$) that is supported by a deep external source

$$J_{lb,M} = -\varphi D_m \frac{\partial M}{\partial z} \tag{4}$$

and because this methane originates from an external source, the DIC and ammonium fluxes at the lower boundary remain equal to zero. This is referred to as the "external methane flux" lower boundary condition. The third and final case is a situation in which there is an internal methane source below the depth of the model lower boundary. We specify the DIC and ammonium fluxes based on equation (2), $r_{N:C}$, and the carbon oxidation state of the organic matter that is degraded in the deep sediments, i.e.,

$$J_{lb,C} = -\varphi D_C \frac{\partial C}{\partial z} = \frac{L_3^{deep}}{L_2^{deep}} J_{lb,M} \tag{5}$$

and

$$J_{lb,N} = -\varphi D_N \frac{\partial N}{\partial z} = \frac{r_{N:C}^{deep}}{L_2^{deep}} J_{lb,M} \tag{6}$$

Table 4. Model Specific Parameters and Description of the Model Runs

	ω (cm yr^{-1})	G_o (mg C gdw^{-1})	k_{OM} (yr^{-1})	$J_{lb,M}$	$J_{lb,C}$ (mol m^{-2} yr^{-1})[a]	$J_{lb,N}$	Key Characteristics of the Model Run
N1[b]	0.067	10	0.003	0	0	0	No methane flux at the lower model boundary, no methane source within the model domain
N2[b]	0.13	22	0.003	0	0	0	No methane flux at the lower model boundary, methane production within the model domain
N3[b]	0.067	10	0.003	−0.20	0	0	Methane flux across lower model boundary from a deep external source without accompanying DIC and ammonium fluxes
N4	0.067	10	0.003	−0.20	−0.14	−0.049	Methane flux across lower model boundary from a deep internal source with accompanying DIC and ammonium fluxes
N5	0.067	10	0.003	−0.20	−0.07	−0.024	Methane flux across lower model boundary from a 1:1 mixture of a deep internal source and a deep external source with accompanying DIC and ammonium fluxes
N6	0.067	2	0.003	−0.20	−0.14	−0.049	Same as model run *N4* but lower G_o value
N7	0.067	5	0.003	−0.20	−0.14	−0.049	Same as model run *N4* but higher G_o value
N8	0.067	10	0.03	−0.20	−0.14	−0.049	Same as model run *N4* but higher k_{OM} value
N9	0.067	10	0.001	−0.20	−0.14	−0.049	Same as model run *N4* but lower k_{OM} value
N10	0.067	10	0.003	−0.20	−0.14	−0.034	Same as model run *N4* but lower $r_{N:C}^{deep}$ (=0.1 versus 0.143 in model run *N4*)

[a]. Positive fluxes are downward (into the sediments).
[b]. For comparison, the model-specific parameters used here in model runs N1, N2 and N3 are identical to those used in the case 1, 2 and 3 model runs, respectively, in *Burdige and Komada* [2011].

[23] This is the "internal methane flux" lower boundary condition. One can think about this situation as one, for example, in which refractory organic matter escapes remineralization in the surface sediments, but is degraded by methanogenesis below the lower boundary of the model in response to increasing temperatures [*Burdige*, 2011]. However, as noted in section 2.1, this may not necessarily be the only explanation for the occurrence of such a deep zone of methanogenesis.

[24] Regardless of the choice of the lower boundary condition for solutes *M*, *C*, and *N*, for solute *S* we specify that $\partial S/\partial z$ goes to zero at the lower boundary. This lower boundary condition assumes that either all sulfate is consumed in the sediments above the lower boundary or that all reactive POC is consumed before complete sulfate reduction.

[25] The five model equations in Table 2 represent a set of coupled, nonlinear differential equations for which there is no analytical solution. A solution to this set of equations was obtained numerically using the method of lines technique with variable grid spacing [*Burdige*, 2011; *Burdige and Komada*, 2011]. In all model calculations, depth is positive downward, and therefore negative fluxes are upward, toward the sediment surface.

[26] Input parameters used in the model runs are listed in Tables 3 and 4. The sediment accumulation rates (ω) we used are within the range of values observed for nearshore to inner continental margin sediments [e.g., *Middelburg et al*., 1997]. The upward methane flux $J_{lb,M}$ (0.2 mol m^{-2} yr^{-1}) is consistent with fluxes reported by *Berelson et al*. [2005] for sediments along the California/Mexican continental margin in water depths less than 1000 m. At these sites on the California/Mexican margin, methane fluxes of this magnitude result in SMT depths that range from ~100 to 200 cm, consistent with our model results (see section 4.3 and, e.g., Figure 1). In contrast, outer continental margin sediments have lower methane fluxes into the SMT and correspondingly deeper SMT depths. For example, at IODP site U11325 on the northern Cascadia Margin (water depth ~2200 m) the methane flux into the SMT is ~0.03 mol m^{-2} yr^{-1} with an SMT depth of ~5 m [*Malinverno and Pohlman*, 2011]. On the Blake Ridge (water depth ~2700 m), methane fluxes into the SMT are <0.01 mol m^{-2} yr^{-1} with an SMT depth of ~20 m [*Borowski et al*., 2000; *Dickens*, 2001; *Burdige*, 2011].

[27] In all model runs, *ox* was set equal to −0.7 [*Burdige and Komada*, 2011], and therefore the

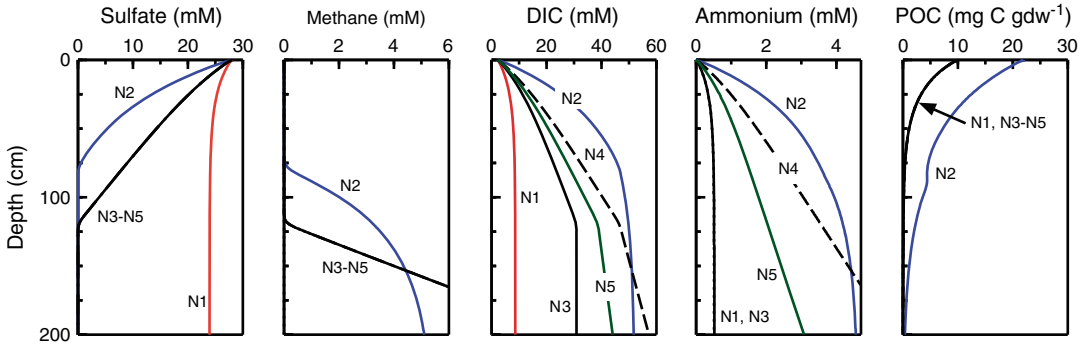

Figure 1. Model-derived sediment pore water profiles and solid phase reactive POC profiles for model runs *N*1–*N*5. The different model parameters and lower boundary conditions for these model runs are described in sections 4.1– 4.3 and in Tables 3 and 4. From 200 cm to the model lower boundary, the model-derived profiles are either constant with depth or continue to increase linearly with depth (as appropriate). Note that the sulfate results for model runs *N*3–*N*5 are identical, as are the methane results (for details see section 4.3). Similarly, the low flux of reactive POC in model run *N*1 (Table 4) results in there being no methane production in these model sediments. Finally, since all of the methane in model run *N*3 is derived from an "external" source (e.g., an ancient gas hydrate) with no concomitant deep source of ammonium, the pore water ammonium profile for model run *N*3 is identical to that for model run *N*1. In both of these cases, the only source of ammonium production is that associated with organic matter remineralization in the surface sediments (i.e., above ~20–30 cm).

expected value of $r_{C:S}$ is 1.7. The organic matter undergoing remineralization in the surface sediments of these model runs was also assumed to have an $r_{N:C}$ value of 0.143 (C:N ratio = 7, which is a "typical" value for marine organic matter). In all but one model run, this same $r_{N:C}$ value was used for the organic matter undergoing remineralization that contributes to the deep internal methane source (see Table 4 and section 4.4 for more details).

[28] In our previous work [*Burdige and Komada*, 2011], we used pore water property-property plots [*Berner*, 1977, 1980] to analyze model results and infer information about remineralization processes occurring in the sediments [also see, for example, similar plots in *Dickens and Snyder*, 2009; *Chatterjee et al.*, 2011]. This approach is based on the observation that a plot of ΔC versus ΔS (where Δ indicates the concentration difference relative to bottom water values) is often linear if DIC production is strongly coupled to bacterial sulfate reduction. The slope of the line through these data ($d\Delta C/d\Delta S$) is related to $r_{C:S}$ according to

$$\frac{d\Delta C}{d\Delta S} = -r_{C:S}\frac{D_s}{D_c} \tag{7}$$

[29] In a similar fashion, sulfate and ammonium concentrations are related to $r_{N:C}$ according to [*Burdige*, 2006]

$$\frac{d\Delta N}{d\Delta S} = -r_{C:S}r_{N:C}\frac{D_s}{D_N} \tag{8}$$

[30] To further examine remineralization processes occurring in these model sediments, we also calculated pore water gradients and diffusive fluxes above and below the SMT. Pore water gradients were calculated using the slopes of the best fit lines through the appropriate linear portions of the model data, and diffusive fluxes were then calculated with Fick's first law [*Burdige*, 2006], using the porosity value and bulk sediment diffusion coefficients given in Table 3.

4. Model Results and Discussion

4.1. No Methane Flux at the Lower Model Boundary, No Methane Source Within the Model Domain

[31] In model run *N*1, POC loading is low (Table 4) and reactive POC is depleted before pore water sulfate, preventing the occurrence of methanogenesis. This model also assumes that there is no upward methane flux at the lower model boundary. Model depth profiles decrease (sulfate or reactive POC) or increase (DIC, ammonium) in exponential-like fashions (Figure 1). These trends are broadly consistent with field results from many nearshore sediments [*Burdige*, 2006]. Applying equations (7) and (8) to property-property plots of the data from this model run returns the input values of $r_{C:S}$ and $r_{N:C}$ [*Burdige and Komada*, 2011].

4.2. No Methane Flux at the Lower Model Boundary, Methane Production Within the Model Domain

[32] Model run *N*2 also uses the "no methane flux" lower boundary condition, but has a higher carbon loading as compared to model run *N*1 (Table 4). This results in complete sulfate depletion in the sediments along with the occurrence of in situ methanogenesis just below the SMT at ~80 cm (Figure 1). Overall, model-derived methane and sulfate profiles are concave up and down, respectively, although the methane gradient just below the SMT and the sulfate gradient just above the SMT are both linear (not shown here, but see Figure 5 in *Burdige and Komada* [2011]). Profiles such as these are also observed in nearshore sediments (see discussions in the beginning of section 2 as well as specific examples in, e.g., *Martens and Berner* [1974], *Alperin et al*. [1992], *Martens et al*. [1992], and *Dale et al*. [2008]). In this model run, ammonium and DIC profiles also are both concave down, due to the production of these solutes in association with sulfate reduction, methanogenesis, and, in the case of DIC, AOM.

[33] In our earlier work [*Burdige and Komada*, 2011], we observed that the ΔC:ΔS property-property plot of these model results returns the value of $r_{C:S}$ for organic matter oxidation coupled to sulfate reduction, despite the occurrence of AOM in the model sediments along with DIC production by methanogenesis. This then led to the important conclusion that the internal cycling of methane by the coupling of in situ methanogenesis and AOM does not lead to deviations in the value of $r_{C:S}$ such as those seen in many continental margin sediments [e.g., *Jahnke*, 1990; *Berelson et al*., 2005]. The simplest explanation for this observation is that the sum of these two reactions (AOM and methanogenesis) is stoichiometrically indistinguishable from sulfate reduction coupled to organic matter oxidation [also see *Jørgensen and Parkes*, 2010], despite the fact that the major zones of methane production and consumption in the sediments are spatially separated.

[34] We now expand this observation to ammonium production in these model sediments. Here we similarly see that a ΔN:ΔS property-property plot using model run *N*2 results returns the $r_{N:C}$ value for sulfate reduction using equation (8) (Figure 2), despite the fact that ~20% of the ammonium in these model sediments is actually produced in association with methanogenesis below the depth of sulfate reduction. A ΔN:ΔC property-property plot with these model results also yields this same value of $r_{N:C}$ (not shown). These observations therefore indicate that the tight coupling between methanogenesis and AOM that "masks" DIC production by methanogenesis in ΔC:ΔS property-property plots [*Burdige and Komada*, 2011] also extends to ammonium production associated with methanogenesis.

4.3. Methane Flux Across Lower Model Boundary From Internal and External Sources, No Methane Production Within the Model Domain

[35] The next three model runs (*N*3–*N*5) have the same reactive POC flux to the sediment surface as model run *N*1 and have pore water ammonium, DIC, and sulfate profiles that show slight curvature near the sediment surface due to the remineralization of this material. At the lower boundary, these three model runs have identical upward methane fluxes, but the fluxes are partitioned into different deep processes/sources (Table 4). These differences result in contrasting DIC and ammonium pore water profiles, particularly at depth.

[36] Because these runs are identical with respect to the POC flux to the sediment surface and the magnitude of the methane flux across the lower model boundary, they have identical methane and sulfate pore water profiles, and in all cases, the SMT is situated at ~120 cm (Figure 1). While the sulfate and methane gradients *into* the SMT appear linear, a careful examination of these profiles *within* the SMT [see *Burdige and Komada*, 2011, Figure 7] indicates that the model profiles show the type of curvature and overlap in this transition zone that is commonly seen in field data [e.g., *Martens and Berner*, 1974; *Reeburgh*, 2007; *Knab et al*., 2008].

[37] Model run *N*3 uses the external methane flux lower boundary condition, where one can think of the methane flux as perhaps coming from a relict gas hydrate deposit with no associated DIC or ammonium flux. Model run *N*4 uses the internal methane flux boundary condition where the methane flux comes from a deep internal source and therefore there are associated DIC and ammonium fluxes. Finally, model run *N*5 represents an intermediate case between *N*3 and *N*4 in which half of the methane comes from an external source and the other half comes from a deep internal source. This division is purely arbitrary, chosen for the sake of this example.

[38] In all three model runs, the DIC profiles are largely linear between the surface zone of organic matter remineralization (upper ~20–30 cm) and the

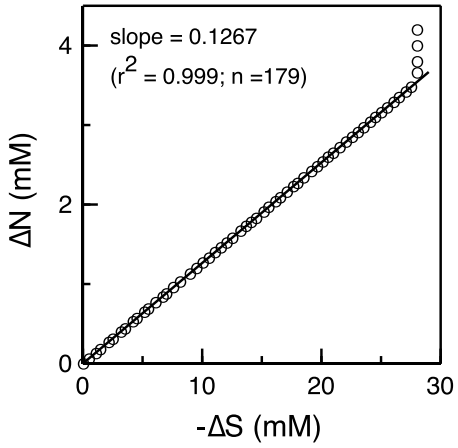

Figure 2. The ΔN:ΔS property-property plot for model run *N*2. Note that only 55 of the ~180 model data points for which $-\Delta S < 28$ m*M* are shown here, to more clearly illustrate the best fit line through the data. Despite the fact that ~20% of the sulfate reduction occurs via AOM rather than organic matter remineralization, and that ~20% of the ammonium is similarly produced in association with methanogenesis rather than sulfate reduction, the value of $r_{N:C}$ determined using equation (8) and a fit to the data where $-\Delta S < 28$ mM (i.e., solely in the zone of sulfate reduction) is identical to the input value of 0.143 (see section 4.2 for details). The data points that deviate from the line where $-\Delta S = 28$ mM represent ammonium that accumulates in the deeper methanogenic sediments in the absence of sulfate.

SMT (Figure 1). The DIC profiles also show an inflection point at the SMT, as seen in field data [*Berelson et al*., 2005; *Harrison et al*., 2009]. The magnitude of the upward DIC flux above the SMT (J_{C+}) as well as the degree of inflection of the profiles in the SMT depends on two quantities: (i) the magnitude of the upward methane flux below the SMT (J_{M-}) which is oxidized to DIC by AOM near the SMT (and which is identical in all three of these model runs), and (ii) the magnitude of the upward DIC flux below the SMT (J_{C-}) from any deep remineralization processes ($N4 > N5 > N3 = 0$). Equally important is the observation that the ratio of the upward DIC and methane fluxes into the SMT from below (J_{C-}/J_{M-}) allows one to distinguish between different sources of methane at depth in these model sediments (Table 5).

[39] For model runs in which there is a deep source of ammonium (model runs *N*4 and *N*5), the ammonium profiles are highly linear below the surface zone of organic matter remineralization and through the SMT into the methane-containing sediments (Figure 1). This is also evidenced by the similarity in the J_{N-} and J_{N+} values for each run (Table 5), and their agreement with the appropriate $J_{lb,N}$ values in Table 4. In addition, linear ammonium profiles only occur when there is deep ammonium production in the sediments, as opposed to the situation in which there is no deep source of ammonium in conjunction with the deep methane source (model run *N*3). The linearity of the ammonium profiles across the SMT in model runs *N*4 and *N*5 coupled with the inflection in the DIC profiles implies that the ammonium:DIC flux ratios above and below the SMT (i.e., J_{N+}/J_{C+} and J_{N-}/J_{C-}) provide complementary information about processes occurring in the sediments. This point is discussed in further detail in section 4.4.

[40] In model run *N*3, the ΔS:ΔC property-property plot shows slight curvature with different slopes (and hence apparent $r_{C:S}$ values) at high and low $-\Delta S$ values [see *Burdige and Komada*, 2011, Figure 8]. This curvature highlights the difficulty in the simple interpretation of such property-property plots when multiple processes affect pore water profiles over differing depth intervals [*Burdige and Komada*, 2011]. For these reasons, in the remainder of the discussion, we will examine pore water gradients and fluxes above and below the SMT as more robust indicators of processes occurring in these model sediments.

[41] For run *N*3, the ratio of the upward DIC flux to the downward sulfate flux above the SMT J_{C+}/J_{S+}) is essentially 1 (Table 5), as predicted by the stoichiometry of AOM in equation (1). For similar reasons, the ratio of the diffusive fluxes of methane and sulfate into the SMT (J_{M-}/J_{S+}) is also 1 (Table 5).

[42] In model run *N*4, the fluxes of methane, DIC, and ammonium at the lower boundary are stochiometrically linked since they originate from deep methanogenesis (see equations (2), (5), and (6)). The upward DIC flux above the SMT (J_{C+}) therefore consists of DIC produced directly by methanogenesis at depth as well as DIC produced by AOM in the SMT when the upward methane flux is oxidized. Since this methane is produced by an internal source, J_{C+}/J_{S+} is again identical to the predicted value of $r_{C:S}$ for DIC production by sulfate reduction (Table 5).

[43] This result further extends our previous observations [*Burdige and Komada*, 2011] that when methane is produced by in situ methanogenesis driven ultimately by the downward burial of organic matter from the sediment surface, the internal recycling of this methane by AOM masks this methanogenesis in certain pore water properties. Specifically here this occurs even if there is large

Table 5. Solute Fluxes (Units: mol m^{-2} yr^{-1}) Above and Below the SMT for Model Run *N*3–*N*10[a]

Fluxes Above the SMT

Model run [b]	J_{S+}	J_{C+}	J_{N+}	J_{C+}:J_{S+}	(pred.) [c]	J_{N+}:J_{C+}	(pred.)[d]
*N*3	0.206	−0.210	n.d.	−1.02	(−1)		
*N*4	0.206	−0.351	−0.050	−1.70	(−1.7)	0.143	(0.143)
*N*5	0.206	−0.280	−0.026	−1.36	(−1.35)	0.092	(0.090)
*N*6	0.200	−0.341	−0.049	−1.70	(−1.7)	0.143	(0.143)
*N*7	0.202	−0.343	−0.049	−1.70	(−1.7)	0.143	(0.143)
*N*8	0.200	−0.340	−0.049	−1.70	(−1.7)	0.143	(0.143)
*N*9	0.251	−0.428	−0.061	−1.71	(−1.7)	0.143	(0.143)
*N*10	0.206	−0.351	−0.036	−1.70	(−1.7)	0.101	(0.1)

Fluxes Below the SMT

Model run	J_{M-}	J_{C-}	J_{N-}	J_C:J_{M-}	(pred.) [e]	J_{N-}:J_{C-}	(pred.) [f]
*N*3	−0.204	0	0				
*N*4	−0.204	−0.143	−0.050	0.70	(0.70)	0.346	(0.346)
*N*5	−0.204	−0.072	−0.025	0.35	(0.35)	0.346	(0.346)
*N*6	−0.204	−0.143	−0.050	0.70	(0.70)	0.346	(0.346)
*N*7	−0.204	−0.143	−0.050	0.70	(0.70)	0.346	(0.346)
*N*8	−0.204	−0.143	−0.050	0.70	(0.70)	0.346	(0.346)
*N*9	−0.236	−0.165	−0.057	0.70	(0.70)	0.347	(0.346)
*N*10	−0.204	−0.143	−0.035	0.70	(0.70)	0.243	(0.242)

Ratios of Fluxes Into the SMT (From Above and Below)

Model run	J_{M-}:J_{S+}	(pred.)
*N*3	−0.99	(−1)
*N*4	−0.99	(−1)
*N*5	−0.99	(−1)
*N*6	−1.02	(−1)
*N*7	−1.01	(−1)
*N*8	−1.02	(−1)
*N*9	−0.94	
*N*10	−0.99	(−1)

[a]Fluxes were calculated as discussed in the text using Fick's first law, and positive fluxes are downward. Pore water gradients above the SMT were determined by linear least squares of the model data from 60–100 cm (*N*3–*N*5 and *N*10), 80–120 cm (*N*6), 75–115 (*N*7), 100–120 (*N*8), and 80–90 cm (*N*9). Below the SMT, this fitting was done with model data from 140–180 cm (*N*3–*N*5 and *N*10), 160–200 cm (*N*6–*N*8), and 120–130 cm (*N*9).

[b]Specific details about the parameters used in each model run can be found in Table 4.

[c]For model run *N*3, the predicted value of $J_{C+}:J_{S+}$ is based on the stoichiometry of AOM (equation (1)). For model runs *N*4 and *N*6–*N*10, it is the value of $r_{C:S}$ for sulfate reduction of C_{org} with a carbon oxidation state of −0.7, given the observed coupling of methanogenesis and AOM "looking" like sulfate reduction (see the text for details). For model run *N*5, the 1:1 split in the sources of the upward flux of methane into these model sediments implies that this predicted ratio is the average of the previous two values.

[d]For model runs *N*4 and *N*6–*N*10, the predicted value of $J_{N+}:J_{C+}$ is the value of $r_{N:C}$ for the C_{org} undergoing remineralization by methanogenesis at depth. For model runs *N*4–*N*9 $r^{deep}_{N:C} = 0.143$ (C:N ratio = 7) while for model run *N*10 $r^{deep}_{N:C} = 0.1$ (C:N ratio = 10). For model run *N*5, the 50:50 split in the sources of the upward flux of methane into the SMT of these model sediments (and the fact that methane derived from an external source is assumed to not have an accompanying ammonium or DIC flux) implies that this predicted ratio is given by

$$\frac{0.5J_{lb,M}r_{N:C}/L_2}{J_{lb,M}(1+0.5L_3/L_2)}$$

where the numerator is the upward flux of ammonium from the deep sediments (see equation (6)) and the denominator is the sum of the upward methane flux (oxidized to DIC by AOM at the SMT) plus the additional upward DIC flux that accompanies deep methane production (see equation (5)).

[e]For model run *N*3, the predicted value of the ratio J_{C-}:J_{M-} is zero since there is no upward DIC flux that accompanies the methane flux. For model runs *N*4 and *N*6–*N*10 the predicted value is L_3/L_2 (see equations (2) or (5)). For model run *N*5, the 1:1 split in the sources of the upward flux of methane and their impact on the upward flux of DIC at depth in these model sediments implies that this predicted ratio is the average of the previous two values.

[f]For model run *N*3, the predicted value of the ratio J_N-:J_C- is zero since there is no upward ammonium flux that accompanies the methane flux. For the remaining model runs, the only process producing DIC and ammonium below the SMT is methanogenesis (see equation (2)). Hence, the predicted value of this ratio is $r^{deep}_{N:C}/L_3$. For model runs *N*4–*N*9 $r^{deep}_{N:C} = 0.143$ (C:N ratio = 7) while for model run *N*10 $r^{deep}_{N:C} = 0.1$ (C:N ratio = 10).

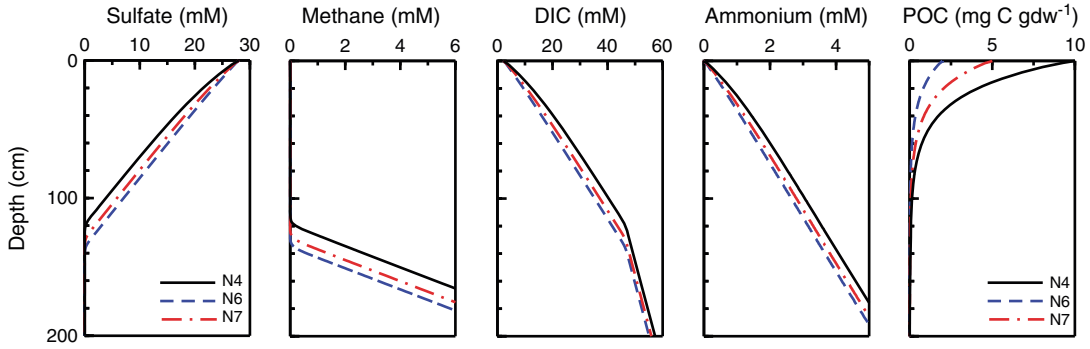

Figure 3. Model-derived sediment pore water profiles and solid phase reactive POC profiles for model runs *N*4, *N6*, and *N*7. As discussed in section 4.4, these three profiles use identical model parameters and lower boundary conditions with the exception of the value for G_o at the sediment surface (see Table 4).

spatial decoupling between the zones of sulfate reduction and methanogenesis. Again, while the model used here does not explicitly define the location of the zone of deep methane production, conceptually, it clearly occurs well below the lower boundary of the model calculations (see section 3 for details).

[44] In a similar fashion, in model run *N*4, the ratio J_{N+}/J_{C+} above the SMT returns the value of $r_{N:C}$ for ammonium production associated with sulfate reduction, despite the fact that ~20% of the ammonium in these model pore waters is actually produced at depth in association with methanogenesis (Table 5). Thus, the linkage between deep methanogenesis and AOM impacts pore water ammonium profiles in the same way that it affects sulfate and DIC profiles, regardless of whether methanogenesis occurs immediately below the SMT (i.e., model run *N*2), or at much greater depths in the sediments as in model run *N*4 (see both model runs in Figure 1).

[45] Finally, for model run *N*5, the ratio J_{C+}/J_{S+} is essentially identical to that predicted when 50% of the DIC is produced by AOM driven by an external methane source, and the remaining 50% produced by what we can think of as "apparent" sulfate reduction, i.e., internal methanogenesis coupled to AOM (Table 5). Similar trends are seen when examining J_{N+}/J_{C+} above the SMT, due to the differing relationship between deep ammonium production and deep methane sources and methanogenesis in this model run (Table 5).

4.4. Linking Surface Remineralization Processes and Deep Reactions

[46] To examine the interplay between organic matter remineralization processes in the surface sediments and deep methanogenesis, we carried out a series of model runs that independently adjusted either G_o (model runs *N*6 and *N*7) or k_{OM} (model runs *N*8 and *N*9) with all other parameters fixed at the values used in model run *N*4 (Table 4).

[47] Figure 3 illustrates the impact on sediment profiles of changing the value of G_o with all other input parameters kept constant at model run *N*4 values. When G_o increases from 2 to 10 mg C gdw^{-1} the depth range over which organic matter remineralization occurs in the surface sediments does not change significantly, because the *e*-folding depth for remineralization is approximately ω/k_{OM} which is constant for all three runs. However, since more sulfate is consumed as G_o increases, the SMT systematically moves upward. Below ~50 cm, all sulfate profiles are linear and essentially parallel to one another since their slopes in this region (J_{S+} in Table 5) are determined by the upward methane flux which is constant in all three model runs (Table 3). Similarly, as G_o increases, the methane profiles also shift upward and are parallel to one another. For DIC and ammonium, increasing G_o increases the amount of curvature in the profiles near the sediment surface, although again below ~50 cm, these profiles are parallel, with (DIC) or without (ammonium) inflection points at the SMT. Fluxes above and below the SMT for model runs *N*6 and *N*7 are therefore essentially the same as those from model run *N*4 (as are their associated flux ratios).

[48] Figure 4 illustrates the impact on sediment profiles of changing the value of k_{OM} with all other input parameters kept constant at model run *N*4 values. Decreasing the value of k_{OM} results in a significant increase in the depth over which organic matter remineralization occurs, since as noted above, the *e*-folding depth for remineralization is roughly given by ω/k_{OM}. However, pore water sulfate depth profiles are impacted

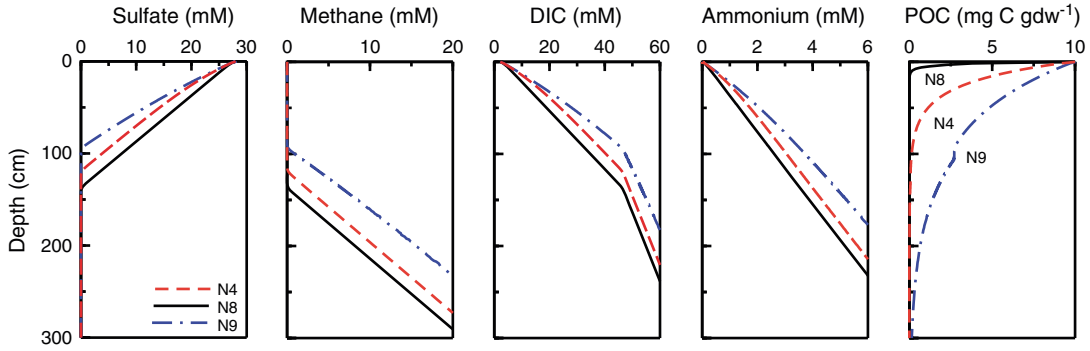

Figure 4. Model-derived sediment pore water profiles and solid phase reactive TOC profiles for model runs *N*4, *N*8, and *N*9. As discussed in section 4.4, these three profiles use identical model parameters and lower boundary conditions with the exception of the value for k_{OM} (see Table 4).

in an opposite sense since decreasing k_{OM} results in the SMT shoaling from ~140 cm (k_{OM} = 0.03 yr^{-1} in model run *N*8) to ~100 cm (k_{OM} = 0.001 yr^{-1} in model run *N*9).

[49] The contrasting responses in sulfate and reactive POC occur in part because diffusive exchange with bottom waters is very effective in replenishing sulfate being consumed near the sediment surface for larger k_{OM} values. In a more general sense, the relationship between k_{OM} and the depth of the SMT seen in Figure 4 can be explained as follows. The downward sulfate gradient (in Figure 5) is given by

$$\frac{S_o - \delta S}{z_{\mathrm{SMT}}} \tag{9}$$

and is constant for a fixed upward methane flux (see Figure 5 for the definition of these symbols). Although a mathematical expression for δS is not easily defined, based on an examination of the original 1-G model for sulfate reduction [e.g., see *Berner*, 1980, equations (6-20)–(6-24)], we might expect δS to increase as k_{OM} decreases. We base this on the fact that in this model, the difference in the sulfate concentration between the sediment surface and the asymptotic value at depth is inversely related to k_{OM} (assuming here that reactive POC rather than sulfate limits sediment sulfate reduction in the 1-G model). As δS increases, the numerator of equation (9) will decrease and in order to maintain a constant sulfate gradient, z_{SMT} must also decrease. Therefore, as k_{OM} decreases, z_{SMT} will decrease. These results are consistent with the model findings of *Meister et al.* [2013] who examined the depth of the SMT as a function of POC reactivity as defined by the reactive continuum [*Boudreau and Ruddick*, 1991] or power law [*Middelburg*, 1989] models.

[50] In these results, we also see that with a decrease in k_{OM} not all of the reactive POC in the surface sediments is consumed by sulfate reduction, and the model results predict that some methanogenesis will occur in the depth region just below the SMT (as opposed to occurring strictly at some greater depth in the sediments below the lower boundary of the model). Evidence for this can be seen in the reactive POC profile of model run *N*9 (k_{OM} = 0.001 yr^{-1}), where significant POC consumption occurs below the SMT (Figure 4). In addition, in this same model run the upward flux of methane into the SMT (J_{M-} = −0.236 mol m^{-2} yr^{-1} in Table 5) exceeds the value of $J_{lb,M}$ in Table 4 (equal to −0.2 mol m^{-2} yr^{-1}), again implying the occurrence of methanogenesis below the SMT but above the lower model boundary in this model run. This occurrence is likely a result of an interplay between (i) changes in the depth scales of POC remineralization by sulfate reduction in the surface sediments, (ii) changes with depth in pore water sulfate concentrations due to this remineralization, and (iii) the sulfate flux needed to oxidize the upward methane flux from depth. For the model conditions used here, the transition between complete and partial consumption of surficial reactive POC by sulfate reduction occurs between k_{OM} values of 0.001 and 0.003 yr^{-1} (i.e., model runs *N*9 and *N*4). However, a more rigorous analysis of this problem would likely indicate that this transition is also a function of a number of other parameters, including $J_{lb,m}$, G_o, and ω.

[51] While model run *N*8 (k_{OM} = 0.03 yr^{-1}) yields fluxes and flux ratios that are essentially identical to those for model run *N*4 (Table 5), the same is not entirely true for model run *N*9 (k_{OM} = 0.001 yr^{-1}). In this model run, the downward sulfate flux into the SMT is greater than that seen in the other model run (0.25 versus ~0.2 mol m^{-2} yr^{-1}; see Table 5) since processes in the SMT now include the direct remineralization of surficial sediment organic matter by sulfate reduction in addition to AOM that results

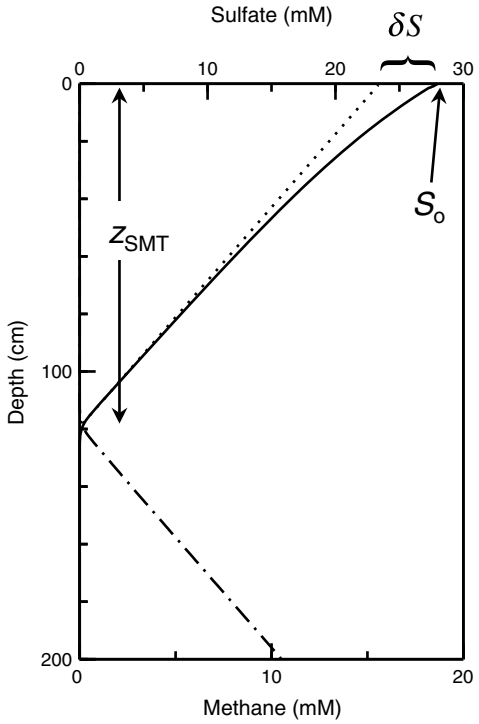

Figure 5. An illustration of the relationship between linear pore water sulfate and methane profiles, and curvature in sulfate profiles near the sediment surface that occurs due to organic matter remineralization in the near-surface sediments. Note that δS is the difference between the bottom water sulfate concentration (S_o) and the sulfate concentration at the sediment surface predicted by extrapolating the linear sulfate gradient to the sediment surface. Since this concentration difference is a function of organic matter remineralization in the near-surface sediments, we suggest that it is inversely related to k_{OM} by analogy with the original 1-G model of *Berner* [1980] (see the text for further details).

from methane production at depth. This occurrence may then also explain why the ratio J_{M-}/J_{S+} is slightly less than 1 in model run *N*9 (Table 5), since some of the sulfate diffusing into the region of the SMT is directly consumed by organic matter remineralization.

4.5. Linking Pore Water Fluxes With the C:N Ratio of Organic Matter Undergoing Remineralization

[52] The highly linear ammonium profiles through the SMT in model runs *N*4–*N*9 as compared to model run *N*3 (Figures 1, 3, and 4) are similar to deep ammonium profiles from continental margin sediments with analogous linear sulfate profiles above the SMT [*Borowski et al*., 1996; *Niewöhner et al*., 1998; *Borowski and Paull*, 2000]. In addition, in shallow sediment profiles (<1 m) from inner continental margin sites [*Bender et al*., 1989; *Prokopenko et al*., 2006; Komada et al., manuscript in preparation], pore water ammonium profiles show gradients that are similar in magnitude to those observed in these model sediments above the SMT (i.e., J_{N+} in Table 5). Overall, this suggests the potential usefulness of the conceptual framework presented here in providing information about remineralization processes occurring in deep marine sediments. The similarity in the values of J_{N-}/J_{C-} for model runs *N*4 and *N*5 is of interest since it provides information strictly about the stoichiometry of methanogenesis in the deep sediments, regardless of whether there is also some methane in the upward flux from an external methane source.

[53] These observations also appear to hold for model run *N*10 (Figure 6), in which we use model parameters that are identical to model run *N*4, but assume that the C:N ratio of the organic matter undergoing methanogenesis at depth is more depleted in nitrogen ($1/r^{deep}_{N:C} = 10$) than that undergoing remineralization in the surface sediments ($1/r_{N:C} = 7$; Table 4). This assumption is not necessarily unreasonable, since more refractory organic matter is generally depleted in nitrogen relative to more reactive organic matter [e.g., *Burdige*, 1991] and organic matter undergoing remineralization at depth in sediments might be expected to be less reactive than that being remineralized near the sediment surface.

[54] In model run *N*10, the ammonium profile is linear through the SMT, and the slope (i.e., the upward ammonium flux) of the model profile (both above and below the SMT) is lower than that of model run *N*4 because of these differences in C:N ratios (Table 4). Again, the values of J_{N-} and J_{N+} agree well with the value of $J_{lb,N}$ for this model run (compare values in Tables 5 and 4).

[55] Application of these model results to field data also requires additional considerations if one wants to use similar fluxes obtained from field data to examine the C:N ratio of the organic matter undergoing remineralization in deep sediments. For example, when the DIC and ammonium fluxes below the SMT for these model runs are taken at face value, their ratio (J_{C-}/J_{N-}) might suggest the remineralization of very nitrogen-rich organic matter at depth in these model sediments (Table 6). In fact, a more accurate representation of the C:N ratio of this material must also account for carbon that is remineralized and partitioned into the upward methane flux (i.e., $(J_{C-} + J_{M-})/J_{N-}$).

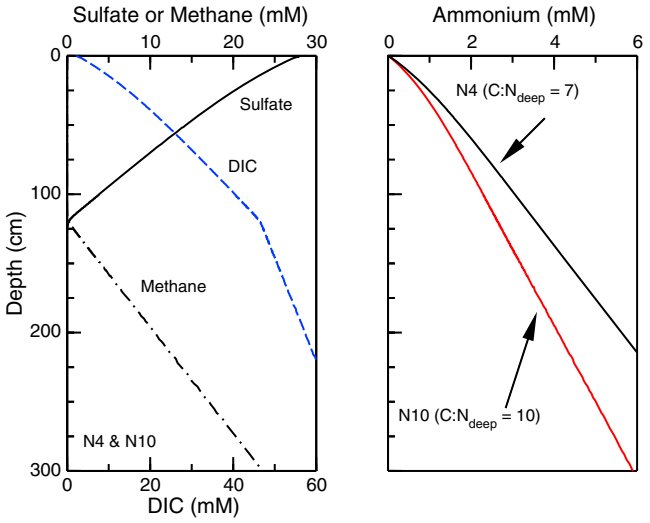

Figure 6. Model-derived sediment pore water profiles for model runs *N*4 and *N*10. As discussed in section 4.5, these profiles use identical model parameters and lower boundary conditions with the exception of the C:N ratio of the organic matter undergoing remineralization in the deep sediments below the lower model boundary ($= 1/r_{N:C}^{deep}$). This results in identical sulfate, DIC, and methane profiles for both model runs, but different ammonium profiles.

[56] At the same time, since this methane flux is oxidized by AOM in the SMT, in model runs *N*4 and *N*6–*N*10, the ratio of the upward DIC and ammonium fluxes just above the SMT (i.e., J_{C+}/J_{N+}) accurately represents the C:N ratio of the organic matter undergoing remineralization at depth (see discussions of similar phenomena in *Burdige and Komada* [2011]). However in model run *N*5, this approach fails because half of the upward methane flux is derived from an ancient source, resulting in a predicted C:N ratio of the organic matter undergoing remineralization at depth that is too carbon rich.

[57] These observations highlight the fact that the correct interpretation of these model observations requires that the results be examined within the context of the conceptual model presented here, paying close attention to sources of methane at depth, and their relationship to deep DIC and ammonium production. Similar considerations also need to be taken into account in the interpretation of analogous fluxes and flux ratios obtained with field pore water data.

Table 6. Predicted C:N Ratio of the Organic Matter Undergoing Remineralization at Depth in the Model Sediments Based on Solute Fluxes as Compared to the Actual Values[a]

Model Run	J_{C-}/J_{N-}	$\frac{J_{C-}+J_{M-}}{J_{N-}}$	J_{C+}/J_{N+}	Actual C:N ratio
*N*4	2.9	7	7	7
*N*5	2.9	11.1	10.9	7
*N*6	2.9	7	7	7
*N*7	2.9	7	7	7
*N*8	2.9	7	7	7
*N*9	2.9	7	7	7
*N*10	4.1	10	9.9	10

[a]All fluxes are taken from Table 5. The actual C:N ratio listed here is $1/r_{N:C}$ for the organic matter undergoing remineralization by methanogenesis at depth (see sections 3 and 4.4 for more details).

5. Conclusions

[58] The results presented here show that pore water ammonium profiles through the SMT represent an independent "tracer" of remineralization processes occurring in deep sediments that complement information obtained from profiles of solutes directly associated with AOM and carbonate precipitation, i.e., DIC, methane, and sulfate. Specifically, linear ammonium profiles through the SMT result from deep ammonium production associated with in situ methanogenesis at depth, while pore water DIC profiles show an inflection point in the SMT based on the type of deep methane source and the presence/absence of accompanying upward DIC fluxes. Overall, these modeling results provide a conceptual framework that illustrates how pore water profiles within the uppermost few meters of the sediment column can be used to obtain important information about remineralization processes and methane sources in deep marine sediments.

[59] However, a complete quantitative interpretation of field pore water data using this modeling approach

also requires the inclusion of carbonate precipitation in model equations such as those presented here. Its occurrence will impact both the shape of the pore water profiles as well as the interpretation of pore water property-property plots and calculated solute diffusive fluxes [e.g., *Berelson et al*., 2005; *Snyder et al*., 2007; *Burdige and Komada*, 2011]. Quantifying carbonate precipitation will require independent results such as pore water Ca^{2+} profiles, as well as isotopic tracers of DIC and/or methane sources [e.g., *Chatterjee et al*., 2011].

Acknowledgments

[60] This work was supported by the following grants from NSF (Chemical Oceanography Program): OCE-115562 (to DJB) and OCE-1155764 (to TK). We thank two anonymous reviewers for providing us with comments that greatly improved an earlier version of this manuscript. We also thank Jerry Dickens, whose review of another of our manuscripts motivated the work presented here.

References

Alperin, M. J., and T. M. Hoehler (2009), Anaerobic methane oxidation by archaea/sulfate-reducing bacteria aggregates: 1. Thermodynamic and physical constraints, *Am. J. Sci.*, *309*, 869–957.

Alperin, M. J., W. S. Reeburgh, and A. H. Devol (1992), Organic carbon remineralization and preservation in sediments of Skan Bay, Alaska, in *Productivity, Accumulation, and Preservation of Organic Matter in Recent and Ancient Sediments*, edited by J. K. Whelan and J. W. Farrington, pp. 99–122, Columbia University Press, New York, NY.

Archer, D., B. Buffett, and P. McGuire (2012), A two-dimensional model of the passive coastal margin deep sedimentary carbon and methane cycles, *Biogeosciences*, *9*, 2859–2878.

Bender, M., R. Jahnke, R. Weiss, W. Martin, D. T. Heggie, J. Orchardo, and T. Sowers (1989), Organic carbon oxidation and benthic nitrogen and silica dynamics in San Clemente Basin, a continental borderland site, *Geochim. Cosmochim. Acta*, *53*, 685–697.

Berelson, W. M., M. Prokopenko, F. J. Sansone, A. W. Graham, J. McManus, and J. M. Bernhard (2005), Anaerobic diagenesis of silica and carbon in continental margin sediments: Discrete zones of TCO2 production, *Geochim. Cosmochim. Acta*, *69*, 4611–4629.

Berner, R. A. (1977), Stoichiometric models for nutrient regeneration in anoxic sediments, *Limnol. Oceanogr.*, *22*, 781–786.

Berner, R. A. (1980), *Early Diagenesis, A Theoretical Approach*, 241 pp., Princeton University Press, Princeton, N.J.

Bohrmann, G., and M. Torres (2006), Gas hydrates in marine sediments, in *Marine Geochemistry*, edited by H. D. Schultz and M. Zabel, pp. 481–512, Springer, Berlin.

Borowski, W. S., and C. K. Paull (2000), Data report: Nitrogen isotopic composition of pore-water ammonium, Blake Ridge, site 997, in *Proceedings ODP, Sci. Results*, edited by C. K. Paull, R. Matsumoto, P. J. Wallace and W. P. Dillon, pp. 171–172, TAMU, College Station, TX.

Borowski, W. S., C. K. Paull, and W. Ussler III (1996), Marine pore-water sulfate profiles indicate in situ methane flux from underlying gas hydrate, *Geology*, *24*, 655.

Borowski, W. S., C. K. Paull, and W. Ussler III (1999), Global and local variations of interstitial sulfate gradients in deep-water, continental margin sediments: Sensitivity to underlying methane and gas hydrates, *Mar. Geol.*, *159*, 131–154.

Borowski, W. S., N. M. Rodriguez, C. K. Paull, and W. Ussler III (2013), Are ^{34}S-enriched authigenic sulfide minerals a proxy for elevated methane flux and gas hydrates in the geologic record?, *Mar. Pet. Geol.*, doi:10.1016/j.marpetgeo.2012.12.009, in press.

Borowski, W. S., T. M. Hoehler, M. J. Alperin, N. M. Rodriquez, and C. K. Paull (2000), Significance of anaerobic methane oxidation in methane-rich sediments overlying the Blake Ridge gas hydrate, in *Proceedings ODP, Sci. Results*, edited by C. K. Paull, R. Matsumoto, P. J. Wallace and W. P. Dillon, pp. 87–99, TAMU, College Station, TX.

Boudreau, B. P. (1997), *Diagenetic Models and Their Implementation*, 414 pp., Springer-Verlag, Berlin.

Boudreau, B. P., and B. R. Ruddick (1991), On a reactive continuum representation of organic matter diagenesis, *Am. J. Sci.*, *291*, 507–538.

Buffett, B., and D. Archer (2004), Global inventory of methane clathrate: Sensitivity to changes in the deep ocean, *Earth Planet. Sci. Lett.*, *227*, 185–199.

Burdige, D. J. (1991), The kinetics of organic matter mineralization in anoxic marine sediments, *J. Mar. Res.*, *49*, 727–761.

Burdige, D. J. (2006), *Geochemistry of Marine Sediments*, 609 pp., Princeton Univ. Press, Princeton.

Burdige, D. J. (2011), The temperature dependence of organic matter remineralization in deeply buried marine sediments, *Earth Planet. Sci. Lett.*, *311*, 396–410.

Burdige, D. J., and T. Komada (2011), Anaerobic oxidation of methane and the stoichiometry of remineralization processes in continental margin sediments, *Limnol. Oceanogr.*, *56*, 1781–1796.

Chatterjee, S., G. R. Dickens, G. Bhatnagar, W. G. Chapman, B. Dugan, G. T. Snyder, and G. J. Hirasaki (2011), Pore water sulfate, alkalinity, and carbon isotope profiles in shallow sediment above marine gas hydrate systems: A numerical modeling perspective, *J. Geophys. Res.*, *116*, B09103.

Claypool, G. E., and I. R. Kaplan (1974), The origin and distribution of methane in marine sediments, in *Natural Gases in Marine Sediments*, edited by I. R. Kaplan, pp. 99–139, Plenum Press, New York.

Claypool, G. E., and K. A. Kvenvolden (1983), Methane and other hydrocarbon gases in marine sediment, *Ann. Rev. Earth Planet. Sci.*, *11*, 299.

Cowie, G. L., and J. I. Hedges (1994), Biochemical indicators of diagenetic alteration in natural organic matter mixtures, *Nature*, *369*, 304–307.

D'Hondt, S., S. Rutherford, and A. J. Spivack (2002), Metabolic activity of subsurface life in deep-sea sediments, *Science*, *295*, 2067–2070.

Dale, A., P. Regnier, N. Knab, B. Jorgensen, and P. Van Cappellen (2008), Anaerobic oxidation of methane (AOM) in marine sediments from the Skagerrak (Denmark): II. Reaction-transport modeling, *Geochim. Cosmochim. Acta*, *72*, 2880–2894.

Devol, A. H., J. J. Anderson, K. Kuivala, and J. W. Murray (1984), A model for coupled sulfate reduction and methane oxidation in the sediments of Saanich Inlet, *Geochim. Cosmochim. Acta*, *48*, 933–1004.

Dickens, G. R. (2001), Sulfate profiles and barium fronts in sediment on the Blake Ridge: Present and past methane fluxes through a large gas hydrate reservoir, *Geochim. Cosmochim. Acta*, *65*, 529–543.

Dickens, G. R., and G. T. Snyder (2009), Interpreting upward methane flux from marine pore water profiles, *Fire In The Ice, Winter*, 7–10.

Froelich, P. N., G. P. Klinkhammer, M. L. Bender, N. A. Luedtke, G. R. Heath, D. Cullen, P. Dauphin, D. Hammond, B. Hartman, and V. Maynard (1979), Early oxidation of organic matter in pelagic sediments of the eastern equatorial Atlantic: Suboxic diagenesis, *Geochim. Cosmochim. Acta*, *43*, 1075–1090.

Goloway, F., and M. Bender (1982), Diagenetic models of interstitial nitrate profiles in deep sea suboxic sediments, *Limnol. Oceanogr.*, *27*, 624–638.

Harrison, B. K., H. Zhang, W. Berelson, and V. J. Orphan (2009), Variations in archaeal and bacterial diversity associated with the sulfate-methane transition zone in continental margin sediments (Santa Barbara Basin, California), *Appl. Environ. Microbiol.*, *75*, 1487–1499.

Hein, J., W. Normark, B. McIntyre, T. Lorenson, and C. Powell (2006), Methanogenic calcite, ^{13}C-depleted bivalve shells, and gas hydrate from a mud volcano offshore southern California, *Geology*, *34*, 109–112.

Henrichs, S. M., and W. S. Reeburgh (1987), Anaerobic mineralization of marine sediment organic matter: Rates and the role of anaerobic processes in the oceanic carbon economy, *Geomicrobiol. J.*, *5*, 191–237.

Hensen, C., and K. Wallmann (2005), Methane formation at Costa Rica continental margin—Constraints for gas hydrate inventories and cross-décollement fluid flow, *Earth Planet. Sci. Lett.*, *236*, 41–60.

Hensen, C., M. Zabel, K. Pfeifer, T. Schwenk, S. Kasten, N. Riedinger, H. D. Schulz, and A. Boetius (2003), Control of sulfate pore-water profiles by sedimentary events and the significance of anaerobic oxidation of methane for the burial of sulfur in marine sediments, *Geochim. Cosmochim. Acta*, *67*, 2631–2647.

Iversen, N., and B. B. Jørgensen (1985), Anaerobic methane oxidation at the sulfate-methane transition in marine sediments from the Kattegat and Skagerrak (Denmark), *Limnol. Oceanogr.*, *30*, 944–955.

Jahnke, R. A. (1990), Early diagenesis and recycling of biogenic debris at the seafloor, Santa Monica Basin, California, *J. Mar. Res.*, *48*, 413–436.

Jørgensen, B. B., and R. J. Parkes (2010), Role of sulfate reduction and methane production by organic carbon degradation in eutrophic fjord sediments (Limfjorden, Denmark), *Limnol. Oceanogr.*, *55*, 1338–1352.

Klump, J. V., and C. S. Martens (1989), The seasonality of nutrient regeneration in an organic rich coastal sediment: Kinetic modelling of changing pore water-nutrient and sulfate distributions, *Limnol. Oceanogr.*, *34*, 559–577.

Knab, N. J., B. A. Cragg, C. Borowski, R. J. Parkes, R. Pancost, and B. B. Jørgensen (2008), Anaerobic oxidation of methane (AOM) in marine sediments from the Skagerrak (Denmark): I. Geochemical and microbiological analyses, *Geochim. Cosmochim. Acta*, *72*, 2868–2879.

Knittel, K., and A. Boetius (2009), Anaerobic oxidation of methane: Progress with an unknown process, *Annu. Rev. Microbiol.*, *63*, 311–334.

Komada, T., D. J. Burdige, S. M. Crispo, E. R. M. Druffel, S. Griffin, L. Johnson, and D. Le (2013), Dissolved organic carbon dynamics in anaerobic sediments of the Santa Monica Basin, *Geochim. Cosmochim. Acta*, 253–273, doi:10.1016/j.gca.2013.02.017.

Kujawinski, E. B. (2011), The impact of microbial metabolism on marine dissolved organic matter, *Ann. Rev. Mar. Sci.*, *3*, 567–599.

Leifer, I., B. P. Luyendyk, J. Boles, and J. F. Clark (2006), Natural marine seepage blowout: Contribution to atmospheric methane, *Global Biogeochem. Cycles*, *20*, GB3008.

Lerman, A. (1977), Migrational processes and chemical reactions in interstitial waters, in *The Sea, Vol. 6*, edited by E. D. Goldberg, I. N. McCave, J. J. O'Brien and J. H. Steele, pp. 695–738, Wiley, New York.

Luff, R., and K. Wallmann (2003), Fluid flow, methane fluxes, carbonate precipitation and biogeochemical turnover in gas hydrate-bearing sediments at Hydrate Ridge, Cascadia Margin: Numerical modeling and mass balances, *Geochim. Cosmochim. Acta*, *67*, 3403–3421.

Malinverno, A., and J. W. Pohlman (2011), Modeling sulfate reduction in methane hydrate-bearing continental margin sediments: Does a sulfate-methane transition require anaerobic oxidation of methane?, *Geochem. Geophys. Geosyst.*, *12*, Q07006.

Martens, C. S., and R. A. Berner (1974), Methane production in the interstitial waters of sulfate-depleted marine sediments, *Science*, *185*, 1167.

Martens, C. S., and J. V. Klump (1980), Biogeochemical cycling in an organic-rich marine basin—1. Methane sediment-water exchange processes, *Geochim. Cosmochim. Acta*, *44*, 471–490.

Martens, C. S., and J. P. Chanton (1989), Radon as a tracer of biogenic gas equilibration and transport from methane saturated sediments, *J. Geophys. Res.*, *94*, 3451–3459.

Martens, C. S., R. I. Haddad, and J. P. Chanton (1992), Organic matter accumulation, remineralization and burial in an anoxic marine sediment, in *Productivity, Accumulation, and Preservation of Organic Matter in Recent and Ancient Sediments*, edited by J. K. Whelan and J. W. Farrington, pp. 82–98, Columbia University Press, New York.

Martens, C. S., D. B. Albert, and M. J. Alperin (1998), Biogeochemical processes controlling methane in gassy coastal sediments—Part 1. A model coupling organic matter flux to gas production, oxidation and transport, *Cont. Shelf Res.*, *18*, 1741–1770.

Martin, W. R., and F. L. Sayles (2003), The recycling of biogenic material at the sea floor, in *Treatise on Geochemistry*, edited by F. T. Machenzie, pp. 367–365, Elsevier, Amsterdam.

Megonigal, J. P., M. E. Hines, and P. T. Visscher (2003), 8.08—Anaerobic metabolism: Linkages to trace gases and aerobic processes, in *Treatise on Geochemistry*, edited by H. D. Holland and K. K. Turekian, pp. 317–424, Pergamon, Oxford.

Meister, P., B. Liu, T. G. Ferdelman, B. B. Jørgensen, and A. Khalili (2013), Control of sulphate and methane distributions in marine sediments by organic matter reactivity, *Geochim. Cosmochim. Acta*, *104*, 183–193.

Meister, P., J. A. McKenzie, C. Vasconcelos, S. Bernasconi, M. Frank, M. Gutjahr, and D. P. Schrag (2007), Dolomite formation in the dynamic deep biosphere: Results from the Peru Margin, *Sedimentol.*, *54*, 1007–1032.

Middelburg, J. J. (1989), A simple rate model for organic matter decomposition in marine sediments, *Geochim. Cosmochim. Acta*, *53*, 1577–1581.

Middelburg, J. J., K. Soetaert, and P. M. J. Herman (1997), Empirical relationships for use in global diagenetic models, *Deep-Sea Res. I*, *44*, 327–344.

Niewöhner, C., C. Hensen, S. Kasten, M. Zabel, and H. D. Schulz (1998), Deep sulfate reduction completely mediated by anaerobic methane oxidation in sediments of the upwelling area off Namibia, *Geochim. Cosmochim. Acta*, *62*, 455–464.

Normark, W., D. Piper, and R. Sliter (2006), Sea level and tectonic control of middle to late Pleistocene turbidite systems in Santa Monica Basin, offshore California, *Sedimentol.*, *53*, 867–897.

Paull, C. K., W. R. Normark, W. Ussler III, D. W. Caress, and R. Keaten (2008), Association among active seafloor deformation, mound formation, and gas hydrate growth and accumulation within the seafloor of the Santa Monica Basin, offshore California, *Mar. Geol.*, *250*, 258–275.

Prokopenko, M. G., D. E. Hammond, W. M. Berelson, J. M. Bernhard, L. Stott, and R. Douglas (2006), Nitrogen cycling in the sediments of Santa Barbara basin and Eastern Subtropical North Pacific: Nitrogen isotopes, diagenesis and possible chemosymbiosis between two lithotrophs (Thioploca and Anammox)—"riding on a glider", *Earth Planet. Sci. Lett.*, *242*, 186–204.

Reeburgh, W. S. (1983), Rates of biogeochemical processes in anoxic sediments, *Annu. Rev. Earth Planet. Sci.*, *11*, 269–298.

Reeburgh, W. S. (2007), Oceanic methane biogeochemistry, *Chem. Rev.*, *107*, 486–513.

Schulz, H. D., and M. Zabel (Eds) (2006), *Marine Geochemistry*, Springer-Verlag, Berlin, 2nd edition, 593 pp.

Snyder, G. T., A. Hiruta, R. Matsumoto, G. R. Dickens, H. Tomaru, R. Takeuchi, J. Komatsubara, Y. Ishida, and H. Yu (2007), Pore water profiles and authigenic mineralization in shallow marine sediments above the methane-charged system on Umitaka Spur, Japan Sea, *Deep-Sea Res. II*, *54*, 1216–1239.

Soetaert, K., P. M. J. Herman, and J. J. Midelburg (1996), A model for early diagenetic processes from the shelf to abyssal depths, *Geochim. Cosmochim. Acta*, *60*, 1019–1040.

Sørensen, J., D. J. Hydes, and T. R. S. Wilson (1984), Denitrification in a deep-sea sediment core from the eastern equatorial Atlantic, *Limnol. Oceanogr.*, *29*, 653–657.

Thauer, R. K., K. Jungermann, and K. Decker (1977), Energy conservation in chemotrophic anaerobic bacteria, *Microbiol. Mol. Biol. Rev.*, *41*, 100.

Wallmann, K., G. Aloisi, M. Haeckel, A. Obzhirov, G. Pavlova, and P. Tishchenko (2006), Kinetics of organic matter degradation, microbial methane generation, and gas hydrate formation in anoxic marine sediments, *Geochim. Cosmochim. Acta*, *70*, 3905–3927.

Wellsbury, P., K. Goodman, T. Barth, B. A. Cragg, S. P. Barnes, and R. J. Parkes (1997), Deep marine biosphere fuelled by increasing organic matter availability during burial and heating, *Nature*, *388*, 573–576.

Wilson, T. R. S., J. Thomson, S. Colley, D. J. Hydes, N. C. Higgs, and J. Sørensen (1985), Early organic diagenesis: The significance of progressive subsurface oxidation fronts in pelagic sediments, *Geochim. Cosmochim. Acta*, *49*, 811–822.

Zeebe, R. E., and D. Wolf-Gladrow (2001), *CO_2 in Seawater: Equilibrium, Kinetics and Isotopes*, Elsevier, Amsterdam.